Synthetic and genetic dimers as quantification ruler for single-molecule counting with PALM

Tim N. Baldering[a], Marina S. Dietz[a], Karl Gatterdam[b], Christos Karathanasis[a], Ralph Wieneke[b], Robert Tampé[b], and Mike Heilemann[a,*]
[a]Single Molecule Biophysics, Institute of Physical and Theoretical Chemistry, Goethe University Frankfurt, 60438 Frankfurt, Germany; [b]Institute of Biochemistry, Goethe University Frankfurt, 60438 Frankfurt, Germany

ABSTRACT How membrane proteins oligomerize determines their function. Superresolution microscopy can report on protein clustering and extract quantitative molecular information. Here, we evaluate the blinking kinetics of four photoactivatable fluorescent proteins for quantitative single-molecule microscopy. We identified mEos3.2 and mMaple3 to be suitable for molecular quantification through blinking histogram analysis. We designed synthetic and genetic dimers of mEos3.2 as well as fusion proteins of monomeric and dimeric membrane proteins as reference structures, and we demonstrate their versatile use for quantitative superresolution imaging in vitro and in situ. We further found that the blinking behavior of mEos3.2 and mMaple3 is modified by a reducing agent, offering the possibility to adjust blinking parameters according to experimental needs.

INTRODUCTION

Membrane proteins respond to extracellular stimuli, organize into complexes, and initiate cellular responses. Their activation through a ligand is often associated with a change in their oligomeric state (Lemmon and Schlessinger, 2010; Alguel *et al.*, 2016). A disorder in the assembly is found in a number of diseases. For example, a distorted monomer-to-dimer ratio of receptor tyrosine kinases is found in carcinogenesis (Sun and Bernards, 2014). To characterize such phenotypes, methods that allow measuring protein oligomerization at the level of single complexes and in intact cells are needed.

Modern fluorescence microscopy techniques provide the sensitivity to detect single molecules (Hohlbein *et al.*, 2010). This allows the study of protein complex compositions, for example, by moni-

toring photobleaching (Ulbrich and Isacoff, 2007; Fricke *et al.*, 2015b; Dietz *et al.*, 2013). However, this requires low labeling densities such that point spread functions (PSFs) of individual fluorophores do not overlap. Superresolution microscopy methods such as single-molecule localization microscopy (SMLM) bring the prerequisites for quantitative analysis with high labeling densities (Sauer and Heilemann, 2017). In SMLM, single fluorescence emission events are separated in time by activating only a small subset of fluorophores and determine their position with high precision (Fürstenberg and Heilemann, 2013; Klein *et al.*, 2014; Turkowyd *et al.*, 2016). Superresolution images are generated from the ensemble of single-molecule coordinates. A variety of methods uses this concept, including stochastic optical reconstruction microscopy (STORM) (Rust *et al.*, 2006), direct STORM (*d*STORM) (Heilemann *et al.*, 2008), and photoactivated localization microscopy (PALM) (Betzig *et al.*, 2006). STORM and *d*STORM use photoswitchable organic fluorophores with high brightness, which are operated as photoswitches in imaging buffers complemented with reducing agents. In PALM, photoactivatable fluorescent proteins (FPs) are genetically coupled to a target protein resulting in high labeling efficiencies and a defined stoichiometry. Ideal FPs for PALM exhibit, among other properties, a high photon budget, fast maturation, efficient photoactivation or –conversion, and no tendency to form clusters or aggregates. Examples that fulfil these criteria are mEos3.2 (Zhang *et al.*, 2012), mMaple3 (McEvoy *et al.*, 2012; Wang *et al.*, 2014), Dendra2 (Chudakov *et al.*, 2007), and PAmCherry (Subach *et al.*, 2009). The photoconversion or –activation of these FPs typically occurs following irradiation with UV light. Hybrid approaches using

Abbreviations used: APS, ammonium persulfate; DCM, dichloromethane; dSTORM, direct stochastic optical reconstruction microscopy; FP, fluorescent protein; LAMA, LocAlization Microscopy Analyzer; MEA, β-mercaptoethylamine; MWCO, molecular weight cut-off; PALM, photoactivated localization microscopy; PBS, phosphate-buffered saline; PSF, point spread function; SEC, size exclusion chromatography; SMLM, single-molecule-localization microscopy; STORM, stochastic optical reconstruction microscopy; TEMED, tetramethylethylenediamine; TIRF, total internal reflection fluorescence; Tris-NTA, Tris-*N*-nitrilotriacetic acid.
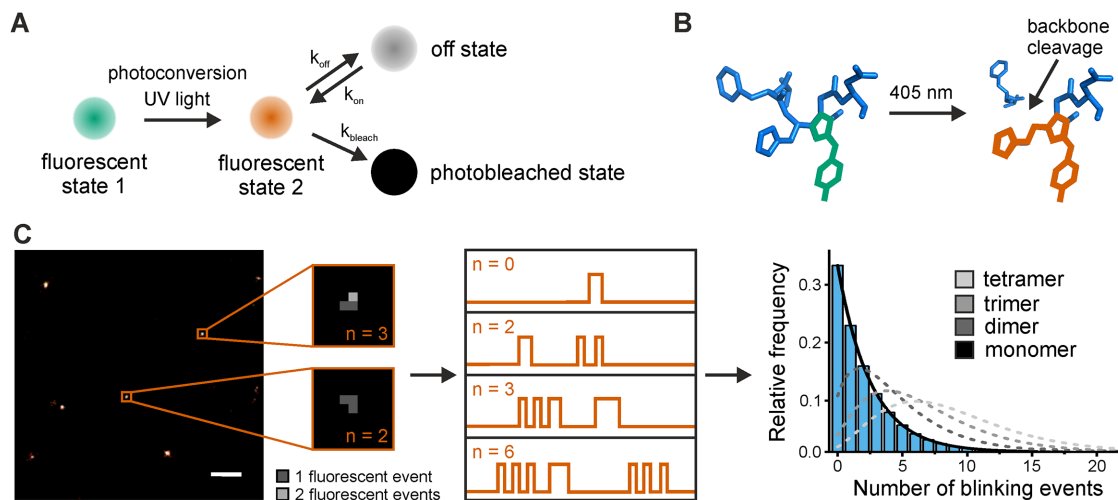
FIGURE 1: Quantitative single-molecule localization microscopy. (A) Basic four-level scheme showing the different states of photoconvertable fluorescent proteins. Fluorescent proteins are photoconverted from a shorter wavelength to a longer wavelength emission state by UV light. Out of the second state, the fluorescent protein can reversibly transit into an off-state (k_{on} and k_{off}) or irreversibly be photobleached (k_{bleach}). (B) Illustration of backbone cleavage of mEos2 after irradiation with UV light. Amino acids Ala60 to Tyr63 of mEos2 are shown. The π-electron system is shown before (green) and after photoconversion (orange). (C) PALM image of single fluorescent spots of mEos3.2, as used for quantitative PALM analysis (scale bar 500 nm) (left). Two selected spots are highlighted and the corresponding zoom images show the number of fluorescent events extracted. Four schematic intensity traces of fluorescent spots and their number of blinking events (n) are shown (middle). From these data, a histogram of the relative frequency of the number of blinking events from all selected regions of interest (ROIs) is generated (right). The blinking number distribution can be approximated with theoretically derived model functions for a monomer (black), dimer (dark gray), trimer (gray), and tetramer (light gray) (these functions were calculated for $p = 0.32$, $q = 0.3$).

both organic fluorophores and photoactivatable FPs for two-color imaging can be a beneficial experimental solution (Muranyi *et al.*, 2013). However, some fluorescent proteins show an increase in their blinking activity in the presence of reducing agents as used in *d*STORM experiments (Endesfelder *et al.*, 2011).

Photoactivatable and –convertible FPs can also be used in quantitative SMLM (Figure 1, A and B), that is, providing superresolution fluorescence images *and* information on protein copy numbers. In its most simple realization, the number of fluorescence emission events from single protein assemblies is extracted (Lee *et al.*, 2012; Puchner *et al.*, 2013; Fricke *et al.*, 2015a). This approach harbors the challenge of under- and overcounting. Undercounting is a consequence of inefficient chromophore maturation. Overcounting can occur if repeated emission events of the same fluorophore occur, called "blinking" (Annibale *et al.*, 2010, 2011a; Durisic *et al.*, 2014). This has been addressed by analyzing the photophysics and blinking behavior of various FPs, and by, for example, extracting dark times to correct for overcounting (Annibale *et al.*, 2011b; Lee *et al.*, 2012). This method minimizes overcounting due to blinking and was used to extract protein densities (Blom *et al.*, 2016; Nasu *et al.*, 2016; van den Berg *et al.*, 2016). However, it requires a fine tuning of the dark time analysis, in order to balance out missed counts on the one hand, and FPs emitting multiple times on the other hand. Still, the dark time analysis underestimates the total number of FPs, since the detection efficiency remains unknown and cannot be extracted.

A simple approach to extract quantitative information from PALM data is to determine the average number of blinking events for a particular FP, and to use that value to determine copy numbers in larger protein complexes (Lando *et al.*, 2012; Endesfelder *et al.*, 2013). An alternative method is the use of pair-correlation functions (Sengupta *et al.*, 2011). Here, the probability of finding a second fluorescence event in a defined distance from a first localized signal is used to analyze larger complexes (Veatch *et al.*, 2012). This approach successfully corrects for overcounting, but again does not consider the detection efficiency and therefore intrinsically leads to undercounting of the true number of FPs. The strength of pair-correlation analysis is to distinguish between clustered and randomly organized molecules, and to determine protein densities and cluster radii (Sherman *et al.*, 2013; Cho *et al.*, 2016; Arnspang *et al.*, 2019). The determination of monomer and dimer fractions in mixed population samples is less straight-forward. In another approach, the blinking kinetics of the fluorophore serve as correction for over- and undercounting (Lee *et al.*, 2012). Here, the probability of blinking contains the kinetic rate constants of on- and off-state transitions. This approach can further be simplified by only counting the blinking events of single fluorophores (Figure 1C). Since blinking is a stochastic process, a sufficient number of spots has to be analyzed in order to obtain appropriate statistics (Hummer *et al.*, 2016). Hence, only this approach determines the average oligomeric state of a particular protein in a cell.

In the simplified blinking analysis, the number of blinking events for an ensemble of single-protein assemblies is histogramed. The distribution is well described by a negative binomial distribution and is characteristic for a particular oligomeric state. By applying a hypergeometric function to the distribution (Eq. 1), the oligomeric state can be determined (Fricke *et al.*, 2015a; Hummer *et al.*, 2016):

$$p_m(n) = \sum_{k=0}^{min(m,n)} \binom{m}{k}\binom{n}{k} q^{m-k}(1-q)^k \, p^{k+1}(1-p)^{n-k} \qquad (1)$$

Here, the fluorophore bleaching probability is described by p, and the fraction of undetected molecules (q) is essential for the description of higher oligomeric systems. The blinking probability can
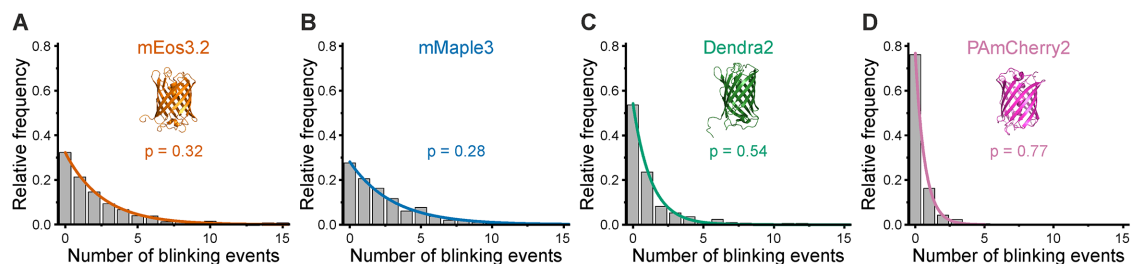
FIGURE 2: Blinking probabilities of four fluorescent proteins. Single-molecule surfaces of fluorescent proteins were imaged with PALM and the data were analyzed quantitatively. The obtained histograms of the number of blinking events of the fluorescent proteins were fitted with a monomer function. The frequency distribution of (A) mEos3.2 showed a p value of 0.32 ($N = 1220$ spots) (crystal structure of mEos2, PDB 3S05), (B) mMaple3 showed a p value of 0.28 ($N = 847$ spots) (no crystal structure available), (C) Dendra2 showed a p value of 0.54 ($N = 420$ spots) (PDB 2VZX), and (D) PAmCherry2 yielded a p value of 0.77 ($N = 1006$ spots) (crystal structure of photoactivated PAmCherry1, PDB 3KCT).

be determined from the p value and is defined as $1 - p$. The number of molecules in an oligomeric system is characterized by $m + 1$ and n displays the number of blinking events where blinking is defined as reoccurrence of fluorescence. This approach of quantitative SMLM was used to determine the oligomeric state of Toll-like receptor 4 in dependency of lipopolysaccharide treatment (Krüger et al., 2017); an extended model was used in combination with the much more complex blinking properties of organic fluorophores (Karathanasis et al., 2017).

In this work, we characterized the blinking probability of four selected FPs commonly used in PALM microscopy. Furthermore, we generated dimeric constructs of mEos3.2 to extract its q value in vitro. Reference membrane proteins (CD86 and CTLA4) were used to determine the p and q values of mEos3.2 in HeLa cells. Finally, we show that the number of blinking events of FPs can be influenced by the reducing agent β-mercaptoethylamine (MEA), which enables adjusting this parameter if needed. In sum, our results extend the toolbox of quantitative SMLM and open the door for new applications in cell biology.

RESULTS AND DISCUSSION

Blinking probabilities of the fluorescent proteins mEos3.2, Dendra2, mMaple3, and PAmCherry2

The blinking properties of single mEos2 were analyzed and described previously (Lee et al., 2012; Avilov et al., 2014). This led to the development of single-protein counting in combination with PALM (Lee et al., 2012; Fricke et al., 2015a, 2017; Hummer et al., 2016). The purpose of this work is to extend the palette of fluores-

cent proteins for quantitative PALM by first analyzing the blinking patterns of four additional FPs that were found useful in PALM imaging experiments, including mEos3.2 (Zhang et al., 2012), mMaple3 (McEvoy et al., 2012; Wang et al., 2014), Dendra2 (Chudakov et al., 2007), and PAmCherry2 (Subach et al., 2009). For that, we deposited the FPs on a poly-L-lysine-coated glass surface at low densities, recorded single-molecule movies and extracted the number of blinking cycles per spot. The data were binned, fitted with a model for a monomeric, blinking fluorophore (Hummer et al., 2016), and p (probability that a FP does not blink) was determined (Figure 2). For mEos3.2, we found a p value of 0.32 ± 0.01 ($R^2 = 0.997$), which is very similar to values reported for mEos2 (Hummer et al., 2016; Krüger et al., 2017). For the other FPs, we found p values of 0.28 ± 0.01 for mMaple3 ($R^2 = 0.990$), 0.54 ± 0.01 for Dendra2 ($R^2 = 0.994$), and 0.77 ± 0.01 for PAmCherry2 ($R^2 = 0.999$) (Table 1). These values translate into an average number of blinking events per fluorophore of 2.1 (mEos3.2), 2.6 (mMaple3), 0.9 (Dendra2), and 0.3 (PAmCherry2), respectively. From this list, PAmCherry2 exhibits the lowest number of blinking cycles per molecule, which is in accordance to previous work on PAmCherry1 using quantitative PALM to determine protein copy numbers in yeast (Lando et al., 2012) or bacteria (Endesfelder et al., 2013; Foo et al., 2015). Dendra2 blinks less often compared with mEos3.2, which fits very well to the data reported by Lee and coworkers comparing mEos2 and Dendra2 (Lee et al., 2012). For mEos3.2 and mMaple3, higher average numbers of blinking events were reported previously (Durisic et al., 2014), which is in accordance with our work.

	p	Fit quality (R^2)	Average number of fluorescence events	Average number of blinking events
mEos3.2	0.32 ± 0.01	0.998	3.1	2.1
mMaple3	0.28 ± 0.01	0.990	3.6	2.6
Dendra2	0.54 ± 0.01	0.994	1.9	0.9
PAmCherry2	0.77 ± 0.01	0.999	1.3	0.3
mEos3.2 (Nikon N-STORM)	0.30 ± 0.01	0.994	3.3	2.3
mEos3.2 + 100 mM MEA	0.17 ± 0.01	0.989	5.9	4.9
mMaple3 + 100 mM MEA	0.56 ± 0.01	0.982	1.8	0.8
CD86-mEos3.2	0.27 ± 0.01	0.997	3.7	2.7

The frequency distributions of the blinking statistics were fitted with hypergeometric fit functions for protein monomers. p describes the bleaching probability of a fluorescent protein. Errors of fits are standard errors of the mean. The fit quality is given by R^2.

TABLE 1: Blinking characteristics of different fluorescent proteins obtained from quantitative SMLM.
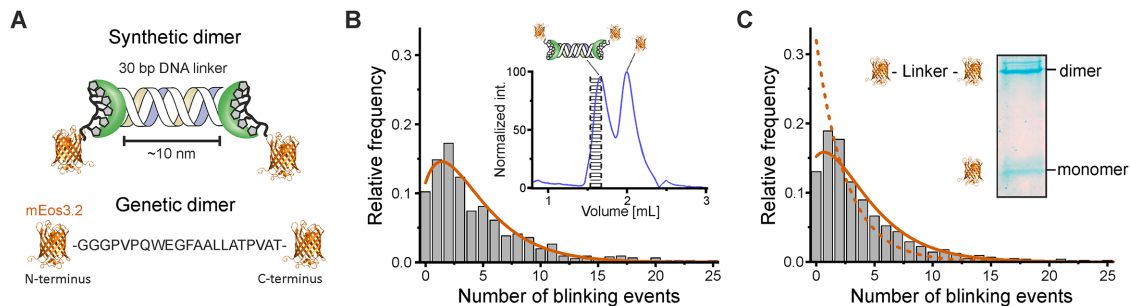
FIGURE 3: Quantitative analysis of synthetic and genetic dimers of mEos3.2. (A) Illustration of the synthetic and genetic dimeric constructs generated in this study. The synthetic dimer connects two mEos3.2 via their His$_6$-tag. A 30–base pair dsDNA with Tris-NTA moieties on both sites serves as a linker. The genetic dimer contains an amino acid linker (GGGPVPQWEGFAALLATPVAT) between two mEos3.2 FPs. (B) Frequency distribution of the number of blinking events of the synthetic dimer construct ($N = 755$ spots). The histogram was fitted with a dimer fit function ($p = 0.32$, $q = 0.36$; orange). Inset: The black dashed lines in the size exclusion chromatogram (blue) indicate the collected fraction of synthetic mEos3.2 dimer used for PALM imaging. (C) Histogram of the genetic mEos3.2 dimer containing a small fraction of monomeric FP ($N = 1058$ spots). The obtained data could be well fitted with a linear combination of monomer and dimer fit function ($p = 0.32$ and $q = 0.36$; orange, solid line) revealing a monomer fraction of 18% ($f = 0.18$). The monomer fit function is shown as an orange dashed line. The SDS gel shows a similar ratio between monomeric and dimeric mEos3.2.

In addition, we analyzed the mean photon counts of all four FPs (Supplemental Figure S1 and Supplemental Table S1). mEos3.2 exhibited the highest average photon budget (1109 photons), while the other three FPs show lower average photon numbers (601, mMaple3; 533, Dendra2; 644, PAmCherry2). This observation can be explained by the used excitation wavelength and emission filter that were optimized for mEos3.2 as well as the lower brightness of mMaple3 (Kaberniuk *et al.*, 2018) and PAmCherry2 (Subach *et al.*, 2009). We also observed higher photon counts for mEos3.2 in comparison to Wang *et al.* (2014), which is due to an excitation wavelength closer to the excitation maximum of mEos3.2.

To demonstrate the general applicability of this method, we compared the results obtained with our home-built microscope to results obtained with a commercial microscope. For this purpose, we determined the blinking parameter p of single mEos3.2 molecules on a surface. Using similar laser intensities, we found a similar value with the commercial microscope ($p = 0.30 \pm 0.01$, Supplemental Figure S2). However, we recommend that these parameters are determined prior to any experimental series on each microscope. To make it more convenient to realize quantitative protein counting from PALM data, we provide a general guideline in the supplementary material.

Synthetic and genetic dimers as calibration references
Next to extending the palette of FPs for single-molecule counting with PALM, we sought to construct dimers of FPs as reference structures for a robust determination of oligomeric states of proteins in complexes. Previous work in the cellular context, used cellular membrane proteins that predominantly are monomeric, or assemble into dimers and trimers (Hummer *et al.*, 2016; Krüger *et al.*, 2017). The purpose of this manuscript is to explore synthetic designs that can serve as reference platform for quantitative PALM. First, we used the blinking probability of monomeric mEos3.2 and simulated the blinking distributions of oligomers by adding up the number of blinking events of two, three, or four spots. The generated histograms were fitted well by linear combinations of the respective fit functions with a percentage of $97.8 \pm 0.8\%$ dimers (Supplemental Figure S3A, left), $91.1 \pm 1.8\%$ trimers (Supplemental Figure S3A, middle), and $85.6 \pm 4.2\%$ tetramers (Supplemental Figure S3A, right). In the next step, we included a q value of 0.3 and

simulated that 30% of dimeric spots contain only one active fluorophore, therefore mimicking incomplete FP maturation (Hummer *et al.*, 2016) (Supplemental Figure S3B). In summary, our simulations demonstrate the reliability of our approach to distinguish between different ratios of monomeric and dimeric data.

To support our simulated data with experimental data, we generated dimeric mEos3.2 constructs following two strategies (Figure 3A). First, we designed a synthetic dimer based on double-stranded DNA as a rigid linker of roughly 10 nm length, equipped with Tris-*N*-nitrilotriacetic acid (Tris-NTA) moieties on both ends (Figure 3A, top, and Supplemental Figure S4). Tris-NTA binds to His-tagged proteins (Hochuli *et al.*, 1987; Lata *et al.*, 2005; Tinazli *et al.*, 2005; Kollmannsperger *et al.*, 2016), and was used as a protein tag in single-molecule superresolution microscopy (Wieneke *et al.*, 2015; Kollmannsperger *et al.*, 2016; Klein *et al.*, 2018). We used this synthetic dimer, conjugated two His$_6$-mEos3.2 to it, and purified the sample with size exclusion chromatography (SEC) (Figure 3B, inset). We recorded single-molecule PALM data, generated a blinking histogram, and found a distribution that is well described with a dimeric fit function assuming that the fraction taken from the SEC run contains only dimerized mEos3.2. The dimeric fit function was applied with the predetermined p value of mEos3.2 (0.32) and allowed us to determine a q value of 0.36 ± 0.03 ($R^2 = 0.960$) (Figure 3B and Table 2). The obtained q for mEos3.2, which describes the fraction of undetected molecules, is slightly higher than the q value of 0.3 obtained for mEos2 in living cells (Hummer *et al.*, 2016). This increase is in accordance with previous work where it was shown that mEos3.2 has a lower detection efficiency than mEos2 (Durisic *et al.*, 2014). Second, we cloned a genetic dimer of two mEos3.2 sequences with an amino acid linker (GGGPVPQWEGFAALLATPVAT) in between using a Hot Fusion reaction as cloning strategy (Figure 3A, bottom; *Materials and Methods*). The dimeric protein was purified by immobilized metal affinity chromatography, attached to a poly-L-lysine–coated glass surface, and single-molecule PALM movies were recorded. From the quantitative SMLM data, we found a mixed distribution with $82.0 \pm 4.5\%$ dimeric and $18.0 \pm 4.5\%$ monomeric mEos3.2 using the previously determined p and q values (Figure 3C and Table 2). This ratio fits to gel chromatography data of the purified dimeric mEos3.2 protein containing a small fraction of

	p	q	Monomer fraction (f)	Fit quality (R^2)
Synthetic mEos3.2 dimer	0.32	0.36 ± 0.03	-	0.960
Genetic mEos3.2 dimer	0.32	0.36	0.180 ± 0.045	0.979
CTLA4-mEos3.2	0.27	0.39 ± 0.01	-	0.994

The frequency distributions of the blinking statistics were fitted with hypergeometric fit functions for protein dimers and mixed populations. p describes the bleaching probability of a fluorescent protein, q the fraction of undetected molecules, and f the fraction of monomers. Errors of fits are standard errors of the mean. The fit quality is given by R^2.

TABLE 2: Fraction of undetected molecules and oligomer ratios of different dimeric samples obtained from quantitative SMLM.

monomeric mEos3.2 (Figure 3C). The quantification of SDS gel bands with GelQuant.NET revealed ~20% monomer and 80% dimer. The monomeric mEos3.2 probably emerged either from inefficient translation or monomeric mEos3.2 plasmid in the Hot Fusion reaction. These results show for the first time that known ratios of monomer and dimer can be determined by our quantitative SMLM approach.

Reducing thiols affect the blinking properties of mEos3.2 and mMaple3

The fluorescence blinking properties of some photomodulatable FPs, including mEos2, were found to change in the presence of the reducing agent β-mercaptoethylamine in phosphate-buffered saline (PBS) buffer (Endesfelder et al., 2011). Following this observation, we hypothesized that this effect will subtly depend on the redox properties of the FP. We therefore explored how MEA-supplemented imaging buffers might influence single-molecule counting. An increased number of blinking cycles would translate into a higher photon budget and a better discrimination between signal and background. We selected mEos3.2 and mMaple3 for this analysis, since these two FPs exhibited the highest number of blinking cycles in PBS buffer. We measured the blinking cycles of mEos3.2 and mMaple3 in PBS supplemented with 100 mM of MEA. For mEos3.2, we found that the average number of blinking events increased substantially from 2.1 to 4.9; p accordingly decreased from 0.32 to 0.17 (Supplemental Figure S5A). This observation is in accordance with mEos2 which shows higher blinking numbers in the presence of MEA (Endesfelder et al., 2011). For mMaple3, we surprisingly found the opposite effect: the number of blinking cycles decreased from 2.6 to 0.8; p increased from 0.28 to 0.56 (Supplemental Figure S5B). The different behavior of these two FPs to a reducing environment can be possibly explained by different theoretical isoelectric points pIs (mEos3.2: 6.95; mMaple3: 8.29, determined with ExPASy ProtParam). Besides, we found that the mean photon counts per activation event of both FPs increased ~20–50% (Supplemental Figure S1, A and B). This exciting result opens a new opportunity of counting two different FPs with qSMLM. So far, FPs tested for this approach have similar spectral properties which prevents their discrimination by, for example, emission spectra. However, sufficiently distinct blinking properties can also serve as a discriminator and allow for a stoichiometry analysis of two FPs.

Monomeric and dimeric membrane proteins as reference structures at the cell membrane

Previously, the quantification of protein oligomerization has been demonstrated with the fluorescent protein mEos2 (Fricke et al., 2015a; Hummer et al., 2016; Krüger et al., 2017). In this work, we investigated four FPs for this purpose, and found that in particular mEos3.2 and mMaple3 are equally suited as mEos2. To support this statement further, we performed experiments in cells using fusion proteins of mEos3.2 with the reference membrane proteins CD86

(monomeric) and CTLA-4 (dimeric). For CD86-mEos3.2, which is predominantly monomeric (Dorsch et al., 2009), we found a p value of 0.27 ± 0.003 ($R^2 = 0.997$), which is only slightly lower than the p value determined in vitro (Supplemental Figure S6A and Table 1). As second reference standard, CTLA-4 was used which is known to occur as dimer in the plasma membrane of human cells (Linsley et al., 1995). Single-molecule PALM data of the fusion protein CTLA-4-mEos3.2 revealed a q value of 0.39 ± 0.01 ($R^2 = 0.994$) (Supplemental Figure S6B and Table 2), which fits to our q value obtained from in vitro SMLM data ($q_{surface} = 0.36$) and confirmed the lower detection efficiency of mEos3.2 compared with mEos2.

In summary, we have extended the palette of photoactivatable and –convertible fluorescent proteins for quantitative PALM experiments. We determined the blinking probabilities of four FPs, and identified mEos3.2 and mMaple3 as suitable for quantitative PALM through blinking distribution analysis. We designed and synthesized dimers of mEos3.2 and demonstrate that they can serve as reference structures for quantitative PALM experiments. Furthermore, we showed that the blinking properties of mEos3.2 and mMaple3 can be influenced by the addition of a reducing agent. We observed an opposite effect for mEos3.2 and mMaple3, which allows tailoring blinking properties and opens new possibilities for multiplexed quantitative SMLM imaging. Finally, we showed that mEos3.2 can be used for quantitative PALM imaging in cells.

MATERIALS AND METHODS
Cloning of plasmids
The DNA sequence of mEos3.2 (pN1-GPI-mEos3.2 [Harwardt et al., 2018]) was amplified by PCR (Bio-Rad C1000 Touch Thermal Cycler) and used for cloning into several plasmids as the pRSET-A vector. For mammalian expression of CD86-mEos3.2 and CTLA4-mEos3.2, mEos2 in the pIRESpuro2 vectors CD86-mEos2 and CTLA4-mEos2 (Fricke et al., 2015a) was replaced by mEos3.2. The mEos3.2 dimer in the pRSET-A vector contains a GGGPVPQWEGFAALLATPVAT linker between the two FPs as in the CD86-mEos3.2 and CTLA4-mEos3.2 constructs. pmMaple3-CAM was a gift from Xiaowei Zhuang (Addgene plasmid #101148; http://n2t.net/addgene:101148; RRID:Addgene_101148). The sequence of monomeric mMaple3 was cloned into the pRSET-A vector. The sequence of Dendra2 was cloned into the pBAD33 vector. All primers, vectors, and the used cloning methods are summarized in Supplemental Table S2. The desired sequences were verified by sequencing. The plasmid containing PAmCherry2 was used in prior studies (Subach et al., 2009).

Expression and purification of fluorescent proteins
Plasmids were electroporated (BTX Havard Apparatus; Gemini System) into *Escherichia coli* BL21-AI cells (Invitrogen) and cultivated on fresh agar plates with appropriate antibiotic. One colony was picked and grown in 10 ml of LB medium in a shaker at 37°C, 200 rpm overnight with the respective antibiotic. LB medium (50–800 ml) was inoculated with 2–10 ml of the preculture and

grown at 30°C, 200 rpm until the cells reached an OD_{600} of 0.35–0.4. Protein expression was induced by adding 50 mM of arabinose (Sigma). The cells were harvested after 120–150 min by centrifugation at 4000 × g for 10 min (Megafuge 1.0, Heraeus). The cells were lysed by sonication (Sonifier 250, Branson Ultrasonics) in 3 ml of lysis buffer (50 mM NaH_2PO_4, 300 mM NaCl; Sigma) containing 10 mM imidazole (Sigma) at pH 8.0. After two centrifugation steps for 15 min at 16,900 × g (Centrifuge 5418 R, Eppendorf), the supernatant was applied onto a Ni-NTA column (Qiagen), washed with lysis buffer containing 20 mM imidazole, and eluted with lysis buffer containing 250 mM imidazole. The buffer was exchanged to PBS (10x DPBS, #14200-067, Life Technologies by Thermo Fisher Scientific) by diluting and concentrating cycles in centrifugal filters with a molecular weight cut-of (MWCO) of 30 kDa (VIVASPIN 6, Sartorius AG) or 100 kDa (Amicon, Sigma). The size of the purified proteins was verified by SDS–PAGE. The separating gel consisted of 0.375 M Tris-HCl, pH 8.8, 0.1% (wt/vol) SDS, 15% acrylamide/bisacrylamide (37:1), 0.05% (wt/vol) ammonium persulfate (APS), and 0.066% tetramethylethylenediamine (TEMED) (Sigma) and the stacking gel of 0.3715 M Tris-HCl, pH 6.8, 0.1% (wt/vol) SDS, 4.3% acrylamide/bisacrylamide (37:1), 0.05% (wt/vol) APS, and 0.1% TEMED. The monomeric and dimeric protein bands were estimated with the GelQuant.NET software provided by biochemlabsolutions.com. The spectral characteristics were analyzed by absorption spectroscopy (Cary 100 UV-VIS Spectrophotometer, Agilent Technologies). mMaple3 was a kind gift from Ulrike Endesfelder (MPI Marburg, Germany).

Generation of the 30–base pair DNA linker
Tris-NTA modification of DNA oligonucleotides. Oligonucleotides with 5′-end NHS-ester modification (Carboxy Modifier C10) on solid support (1 μmol scale) were purchased from Biomers.net GmbH. Cyclam-Glu-Tris-NTA (Lata *et al.*, 2005; Gatterdam *et al.*, 2018) (3 mg; 2.8 μmole) was dissolved in 10% diisopropylethylamine (DIPEA) in dichloromethane $(DCM)_{dry}$. After 2 h reaction at 55°C, the resin was washed 3x with DCM.

For cleavage, the solid was incubated with 500 μl of 32% ammonia at 55°C for 2 h. The solvent was evaporated with a Speedvac (Thermo Fisher Scientific). Tris-NTA modified oligonucleotides were purified by semi-preparative RP-HPLC (mobile phase A: 0.1 M TEAA pH 7.0, B: ACN; gradient 5–20% B in 30 min; MZ-PerfectSil, 300 ODS, 5 μm, 250 × 10 mm, flow 4 ml/min).

Assembly of complementary Tris-NTA-DNA oligonucleotides. A complementary pair of purified Tris-NTA-DNA strands was mixed stoichiometrically to a final concentration of 15 μM using TMg buffer (20 mM Tris, 12.5 mM $MgCl_2$, pH 7.6). Assembly of duplex DNA was assisted with the following temperature program: 20–85°C; heating rate 1°C/min, hold 5 min at 85°C; 85–10°C; cooling rate 1°C/min; 10–85°C; heating rate 1°C/min, hold 5 min at 85°C; 85–20°C; cooling rate 1°C/min.

Assembled Tris-NTA-modified DNA linker was purified 1.5 h after finishing the temperature program by semi-preparative IP-RP-HPLC (mobile phase A: 0.1 M TEAA pH 7.0, B: ACN; gradient 5–20% B in 30 min; MZ-PerfectSil C_{18}, 300 ODS, 5 μm, 250 × 10 mm, flow 4 ml/min). The solvent was evaporated with a Speedvac.

Ni-loading of DNA linker tools. The Tris-NTA chelator compound was dissolved in TMg buffer. After 1 h incubation at ambient temperature, the excess of Ni(II) was separated by ultraflitration (Amicon Ultra-0.5 ml; 3, 10 kDa MWCO).

Native PAGE. The 30–base pair DNA linker was analyzed by nPAGE regarding duplex assembly and purity. Gel solution was prepared by mixing 2.4 ml TBMg (5x) (200 mM Tris, 100 mM boric acid, 62.5 mM $Mg(OAc)_2$, pH 8.0), 2.1 ml H_2O, 7.5 ml acrylamide (Rotiphorese Gel 30), 10 μl TEMED, and 100 μl APS. The solution was filled into a casting stand followed by comb assembly. After polymerization the samples (1 μM) were mixed with orange DNA loading dye (6x) (Thermo Fisher Scientific) and applied to the gel. The O'GeneRuler Ultra Low Range DNA ladder was used as a marker. Gel electrophoresis was performed in TBMg (1x) buffer at 200 V for 1–2 h at ambient temperature. For staining, SYBR Gold (Thermo Fisher Scientific) was diluted 1/10,000 (vol/vol) in the corresponding running buffer. Gels were stained for 5–15 min followed by UV-Vis light detection.

Fluorescence size exclusion chromatography. For analytics and preparative isolation of dimeric complexes, the DNA linker and the His-tagged protein were mixed in the corresponding ratios and incubated for 30–60 min at 4°C. Samples were injected by an auto sampler of the Shimadzu HPLC (LC20AD) system, which was equipped with a Superdex 200 Increase 3.2/300 column (GE Healthcare).

Preparation of single-molecule surfaces of fluorescent proteins
Cover glasses (35 × 64 mm, # 1.5, Thermo Fisher Scientific) were washed in 2-propanol (VWR Chemicals) for 20 min, plasma-cleaned with nitrogen for 15 min (Diener Electronic GmbH) and covered with 100 μg/ml poly-L-lysine (Sigma) for 2 h. flexiPERM chambers (Sarstedt) were placed on the coated cover glasses and the particular fluorescent protein (200 pM–10 nM) in PBS was transferred into the chambers and incubated for 30 min at ambient temperature. The chambers were washed 3x with sterile-filtered PBS before PALM movies were recorded in pure sterile-filtered PBS buffer or supplemented with 100 mM MEA at pH 7.8.

SMLM sample preparation of transfected HeLa cells
HeLa cells (Institut für angewandte Zellkultur, Munich, Germany) were cultivated at 37°C and 5% CO_2 in an automatic CO_2 incubator (Model C 150; Binder GmbH). Cells were transfected with Lipofectamine 3000 (Invitrogen) in six-well plates according to the manufacturers protocol at low DNA concentrations (100 ng/well) one day after seeding the cells in DMEM (Thermo Scientific) supplemented with 1% Glutamax (Thermo Scientific), 100 U/ml penicillin, 100 μg/ml streptomycin (Thermo Scientific), and 10% fetal bovine serum (FBS, Thermo Scientific). 24 h after transfection, cells were scraped, transferred into flexiPERM chambers (Sarstedt) on plasma-cleaned PLL-PEG-RGD surfaces and fixed after another 24 h with PBS containing 4% formaldehyde (Thermo Scientific), 0.2% glutaraldehyde (Sigma), and 400 mM sucrose (Sigma) for 15 min. Finally, the chambers were washed 3x with sterile-filtered PBS.

SMLM measurements
PALM was performed using a home-built widefield setup equipped with an inverted microscope (Olympus IX71) using lasers coupled into a 100x oil immersion objective (PlanApo 100 × TIRFM, NA≥1.45, Olympus), a nose piece for drift minimization and total internal reflection fluorescence (TIRF) mode (Fricke *et al.*, 2015a). Fluorescent proteins were photoconverted or photoactivated by increasing intensities of UV light (405 nm laser, LBX-405-50-CSB-PP, Oxxius, 0–30 mW/cm²) and simultaneously excited with a 568 nm laser (0.21 kW/cm²; Sapphire 568 LP, Coherent). The emission light was filtered using a bandpass filter (BrightLine HC 590/20, AHF). SMLM

movies of 12,000–80,000 frames were recorded with an EMCCD camera (iXon Ultra, Andor) with a physical pixel size of 157 nm (camera pixel and magnification), an exposure time of 100 ms and an EM gain of 200 until almost no blinking was observed. For each sample a minimum of four movies from at least two different measuring days were used for data analysis.

For comparison, SMLM experiments with mEos3.2 were also performed on a commercial microscope (N-STORM, Nikon) (Figure S2). The microscope was equipped with an 100x objective (100 × Apo TIRF oil, 1.49 NA), a 561 nm laser (0.2 kW/cm^2), and a 405 nm laser (0-38 mW/cm^2), and was operated in TIRF mode. Image acquisition was controlled by Micro-Manager and NIS-Elements using an exposure time of 100 ms and an EM gain of 200. SMLM movies were recorded with an EMCCD camera (DU-897U-CS0-BV; Andor Technology, Belfast,UK), using a physical pixel size (camera and magnification) of 158 nm. Recorded movies had a length of 18,000–54,000 frames.

SMLM data analysis
SMLM data analysis was performed as described before (Fricke *et al.*, 2015a; Hummer *et al.*, 2016). PALM movies were analyzed with rapidSTORM (v3.3) (Wolter *et al.*, 2012) by applying an intensity threshold of 63 photons and a PSF full width half maximum of 360 nm. The localization files were tracked with a distance threshold of 90 nm and a trace filter was applied discarding localizations that only appeared in one frame to eliminate background signal. LocAlization Microscopy Analyzer (LAMA) (Malkusch and Heilemann, 2016) was used to generate an image showing the number of fluorescent bursts related to the detected spots. Single spots were selected according to their intensity, shape, and distance to other spots before and after tracking and tracing. The number of blinking events of selected localizations and clusters were extracted from the LAMA image. Further data analysis was performed in OriginPro 2017G (v9.40, OriginLab). Histograms of blinking events were plotted and fitted with the hypergeometric functions yielding the bleaching probability (p), the fraction of undetected molecules (q), and the linear combination weighting factor (f). Values are given with their respective standard errors of the mean.

REFERENCES
Alguel Y, Cameron AD, Diallinas G, Byrne B (2016). Transporter oligomerization. Form and function. Biochem Soc Trans 44, 1737–1744.

Annibale P, Scarselli M, Kodiyan A, Radenovic A (2010). Photoactivatable fluorescent protein mEos2 displays repeated photoactivation after a long-lived dark state in the red photoconverted form. J Phys Chem Lett 1, 1506–1510.

Annibale P, Vanni S, Scarselli M, Rothlisberger U, Radenovic A (2011a). Identification of clustering artifacts in photoactivated localization microscopy. Nat Methods 8, 527–528.

Annibale P, Vanni S, Scarselli M, Rothlisberger U, Radenovic A (2011b). Quantitative photo activated localization microscopy. Unraveling the effects of photoblinking. PLoS One 6, e22678.

Arnspang EC, Sengupta P, Mortensen KI, Jensen HH, Hahn U, Jensen EBV, Lippincott-Schwartz J, Nejsum LN (2019). Regulation of plasma membrane nanodomains of the water channel aquaporin-3 revealed by fixed and live photoactivated localization microscopy. Nano Lett 19, 699–707.

Avilov S, Berardozzi R, Gunewardene MS, Adam V, Hess ST, Bourgeois D (2014). In cellulo evaluation of phototransformation quantum yields in fluorescent proteins used as markers for single-molecule localization microscopy. PLoS One 9, e98362.

Betzig E, Patterson GH, Sougrat R, Lindwasser OW, Olenych S, Bonifacino JS, Davidson MW, Lippincott-Schwartz J, Hess HF (2006). Imaging intracellular fluorescent proteins at nanometer resolution. Science 313, 1642–1645.

Blom H, Bernhem K, Brismar H (2016). Sodium pump organization in dendritic spines. Neurophotonics 3, 41803.

Cho W-K, Jayanth N, English BP, Inoue T, Andrews JO, Conway W, Grimm JB, Spille J-H, Lavis LD, Lionnet T, Cisse II (2016). RNA polymerase II cluster dynamics predict mRNA output in living cells. Elife 5, e13617.

Chudakov DM, Lukyanov S, Lukyanov KA (2007). Using photoactivatable fluorescent protein Dendra2 to track protein movement. BioTechniques 42, 553, 555, 557 passim.

Dietz MS, Haße D, Ferraris DM, Göhler A, Niemann HH, Heilemann M (2013). Single-molecule photobleaching reveals increased MET receptor dimerization upon ligand binding in intact cells. BMC Biophys 6, 6.

Dorsch S, Klotz K-N, Engelhardt S, Lohse MJ, Bünemann M (2009). Analysis of receptor oligomerization by FRAP microscopy. Nat Methods 6, 225–230.

Durisic N, Laparra-Cuervo L, Sandoval-Álvarez A, Borbely JS, Lakadamyali M (2014). Single-molecule evaluation of fluorescent protein photo-activation efficiency using an in vivo nanotemplate. Nat Methods 11, 156–162.

Endesfelder U, Finan K, Holden SJ, Cook PR, Kapanidis AN, Heilemann M (2013). Multiscale spatial organization of RNA polymerase in Escherichia coli. Biophys J 105, 172–181.

Endesfelder U, Malkusch S, Flottmann B, Mondry J, Liguzinski P, Verveer PJ, Heilemann M (2011). Chemically induced photoswitching of fluorescent probes–a general concept for super-resolution microscopy. Molecules 16, 3106–3118.

Foo YH, Spahn C, Zhang H, Heilemann M, Kenney LJ (2015). Single cell super-resolution imaging of E. coli OmpR during environmental stress. Integr Biol (Camb) 7, 1297–1308.

Fricke F, Beaudouin J, Eils R, Heilemann M (2015a). One, two or three? Probing the stoichiometry of membrane proteins by single-molecule localization microscopy. Sci Rep 5, 14072.

Fricke F, Beaudouin J, Malkusch S, Eils R, Heilemann M (2017). Quantitative single-molecule localization microscopy (qSMLM) of membrane proteins based on kinetic analysis of fluorophore blinking cycles. Methods Mol Biol 1663, 115–126.

Fricke F, Dietz MS, Heilemann M (2015b). Single-molecule methods to study membrane receptor oligomerization. Chemphyschem 16, 713–721.

Fürstenberg A, Heilemann M (2013). Single-molecule localization microscopy-near-molecular spatial resolution in light microscopy with photoswitchable fluorophores. Phys Chem Chem Phys 15, 14919–14930.

Gatterdam K, Joest EF, Gatterdam V, Tampé R (2018). The scaffold design of trivalent chelator heads dictates affinity and stability for labeling His-tagged proteins in vitro and in cells. Angew Chem Int Ed Engl 57, 12395–12399.

Harwardt M-LIE, Dietz MS, Heilemann M, Wohland T (2018). SPT and imaging FCS provide complementary information on the dynamics of plasma membrane molecules. Biophys J 114, 2432–2443.

Heilemann M, van de Linde S, Schüttpelz M, Kasper R, Seefeldt B, Mukherjee A, Tinnefeld P, Sauer M (2008). Subdiffraction-resolution fluorescence imaging with conventional fluorescent probes. Angew Chem Int Ed Engl 47, 6172–6176.

Hochuli E, Döbeli H, Schacher A (1987). New metal chelate adsorbent selective for proteins and peptides containing neighbouring histidine residues. J Chromatogr 411, 177–184.

Hohlbein J, Gryte K, Heilemann M, Kapanidis AN (2010). Surfing on a new wave of single-molecule fluorescence methods. Phys Biol 7, 31001.

Hummer G, Fricke F, Heilemann M (2016). Model-independent counting of molecules in single-molecule localization microscopy. Mol Biol Cell 27, 3637–3644.

Kaberniuk AA, Mohr MA, Verkhusha VV, Snapp EL (2018). moxMaple3. A photoswitchable fluorescent protein for PALM and protein highlighting in oxidizing cellular environments. Sci Rep 8, 14738.

Karathanasis C, Fricke F, Hummer G, Heilemann M (2017). Molecule counts in localization microscopy with organic fluorophores. Chemphyschem 18, 942–948.

Klein A, Hank S, Raulf A, Joest EF, Tissen F, Heilemann M, Wieneke R, Tampé R (2018). Live-cell labeling of endogenous proteins with nanometer precision by transduced nanobodies. Chem Sci 9, 152.

Klein T, Proppert S, Sauer M (2014). Eight years of single-molecule localization microscopy. Histochem Cell Biol 141, 561–575.

Kollmannsperger A, Sharei A, Raulf A, Heilemann M, Langer R, Jensen KF, Wieneke R, Tampé R (2016). Live-cell protein labelling with nanometre precision by cell squeezing. Nat Commun 7, 10372.

Krüger CL, Zeuner M-T, Cottrell GS, Widera D, Heilemann M (2017). Quantitative single-molecule imaging of TLR4 reveals ligand-specific receptor dimerization. Sci Signal 10, eaan1308.

Lando D, Endesfelder U, Berger H, Subramanian L, Dunne PD, McColl J, Klenerman D, Carr AM, Sauer M, Allshire RC, *et al.* (2012). Quantitative single-molecule microscopy reveals that CENP-A(Cnp1) deposition occurs during G2 in fission yeast. Open Biol 2, 120078.

Lata S, Reichel A, Brock R, Tampé R, Piehler J (2005). High-affinity adaptors for switchable recognition of histidine-tagged proteins. J Am Chem Soc 127, 10205–10215.

Lee S-H, Shin JY, Lee A, Bustamante C (2012). Counting single photoactivatable fluorescent molecules by photoactivated localization microscopy (PALM). Proc Natl Acad Sci USA 109, 17436–17441.

Lemmon MA, Schlessinger J (2010). Cell signaling by receptor tyrosine kinases. Cell 141, 1117–1134.

Linsley PS, Nadler SG, Bajorath J, Peach R, Leung HT, Rogers J, Bradshaw J, Stebbins M, Leytze G, Brady W, *et al.* (1995). Binding stoichiometry of the cytotoxic T lymphocyte-associated molecule-4 (CTLA-4). J Biol Chem 270, 15417–15424.

Malkusch S, Heilemann M (2016). Extracting quantitative information from single-molecule super-resolution imaging data with LAMA—LocAlization Microscopy Analyzer. Sci Rep 6, 34486.

McEvoy AL, Hoi H, Bates M, Platonova E, Cranfill PJ, Baird MA, Davidson MW, Ewers H, Liphardt J, Campbell RE (2012). mMaple. A photoconvertible fluorescent protein for use in multiple imaging modalities. PLoS One 7, e51314.

Muranyi W, Malkusch S, Müller B, Heilemann M, Kräusslich H-G (2013). Super-resolution microscopy reveals specific recruitment of HIV-1 envelope proteins to viral assembly sites dependent on the envelope C-terminal tail. PLoS Pathog 9, e1003198.

Nasu Y, Benke A, Arakawa S, Yoshida GJ, Kawamura G, Manley S, Shimizu S, Ozawa T (2016). In situ characterization of Bak clusters responsible for cell death using single molecule localization microscopy. Sci Rep 6, 27505.

Puchner EM, Walter JM, Kasper R, Huang B, Lim WA (2013). Counting molecules in single organelles with superresolution microscopy allows tracking of the endosome maturation trajectory. Proc Natl Acad Sci USA 110, 16015–16020.

Rust MJ, Bates M, Zhuang X (2006). Sub-diffraction-limit imaging by stochastic optical reconstruction microscopy (STORM). Nat Methods 3, 793–795.

Sauer M, Heilemann M (2017). Single-molecule localization microscopy in eukaryotes. Chem Rev 117, 7478–7509.

Sengupta P, Jovanovic-Talisman T, Skoko D, Renz M, Veatch SL, Lippincott-Schwartz J (2011). Probing protein heterogeneity in the plasma membrane using PALM and pair correlation analysis. Nat Methods 8, 969–975.

Sherman E, Barr V, Samelson LE (2013). Super-resolution characterization of TCR-dependent signaling clusters. Immunol Rev 251, 21–35.

Subach FV, Patterson GH, Manley S, Gillette JM, Lippincott-Schwartz J, Verkhusha VV (2009). Photoactivatable mCherry for high-resolution two-color fluorescence microscopy. Nat Methods 6, 153–159.

Sun C, Bernards R (2014). Feedback and redundancy in receptor tyrosine kinase signaling. Relevance to cancer therapies. Trends Biochem Sci 39, 465–474.

Tinazli A, Tang J, Valiokas R, Picuric S, Lata S, Piehler J, Liedberg B, Tampé R (2005). High-affinity chelator thiols for switchable and oriented immobilization of histidine-tagged proteins. A generic platform for protein chip technologies. Chemistry 11, 5249–5259.

Turkowyd B, Virant D, Endesfelder U (2016). From single molecules to life. Microscopy at the nanoscale. Anal Bioanal Chem 408, 6885–6911.

Ulbrich MH, Isacoff EY (2007). Subunit counting in membrane-bound proteins. Nat Methods 4, 319–321.

van den Berg J, Galbiati H, Rasmussen A, Miller S, Poolman B (2016). On the mobility, membrane location and functionality of mechanosensitive channels in Escherichia coli. Sci Rep 6, 32709.

Veatch SL, Machta BB, Shelby SA, Chiang EN, Holowka DA, Baird BA (2012). Correlation functions quantify super-resolution images and estimate apparent clustering due to over-counting. PLoS One 7, e31457.

Wang Y, Moffitt JR, Dempsey GT, Xie XS, Zhuang X (2014). Characterization and development of photoactivatable fluorescent proteins for single-molecule-based superresolution imaging. Proc Natl Acad Sci USA 111, 8452–8457.

Wieneke R, Raulf A, Kollmannsperger A, Heilemann M, Tampé R (2015). SLAP. Small labeling pair for single-molecule super-resolution imaging. Angew Chem Int Ed Engl 54, 10216–10219.

Wolter S, Löschberger A, Holm T, Aufmkolk S, Dabauvalle M-C, van de Linde S, Sauer M (2012). rapidSTORM. Accurate, fast open-source software for localization microscopy. Nat Methods 9, 1040–1041.

Zhang M, Chang H, Zhang Y, Yu J, Wu L, Ji W, Chen J, Liu B, Lu J, Liu Y, *et al.* (2012). Rational design of true monomeric and bright photoactivatable fluorescent proteins. Nat Methods 9, 727–729.